DC Arc-Fault Detection Based on Empirical Mode Decomposition of Arc Signatures and Support Vector Machine

Wenchao Miao, Qi Xu, K. H. Lam, Philip W. T. Pong, *Senior Member, IEEE*, and H. Vincent Poor, *Life Fellow, IEEE*

***Abstract*—Protection devices are extensively utilized in direct current (DC) systems to ensure their normal operation and safety. However, series arc faults that establish current paths in the air between conductors introduce arc impedance to the system. Consequently, they can result in a decrease of current, and thus conventional protection devices may not be triggered. Undetected series arc faults can cause malfunctions and even lead to fire hazards. Therefore, a series arc-fault detection system is essential to DC systems to operate reliably and efficiently. In this paper, a series arc-fault detection system based on arc time-frequency signatures extracted by a modified empirical mode decomposition (EMD) technique and using a support vector machine (SVM) algorithm in decision making is proposed for DC systems. The oscillatory frequencies from the arc current are decomposed by the EMD with an analysis of the Hurst exponent (*H*) to reject interference from the power electronics noise. *H* analyzes the trend of a signal and the intrinsic oscillations of the signal are those with values of *H* larger than 1/2. Comparing to traditional filters or wavelet transforms, this method does not require knowledge of the frequency range of the interference which varies from system to system. The capability and applicability of the proposed technique are validated in a photovoltaic system. The effectiveness of arc-fault detection is significantly improved by this technique because it can acquire sufficient and accurate arc signatures and it does not need to predefine various thresholds.**

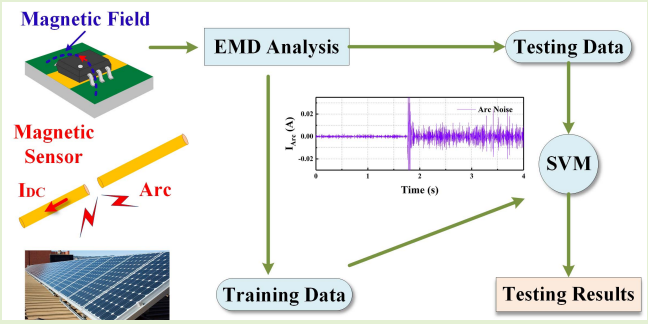

***Index Terms*— Arc fault, arc time-frequency signatures, empirical mode decomposition, support vector machine.**

I. Introduction

DIRECT current (DC) systems are prevalent since they have the characteristics of higher efficiency, better sustainability, less complication, and lower cost compared to alternating current (AC) systems [1], [2]. The continuous development of distributed renewable energy sources, electrical vehicles, storage devices, and DC loads are contributing to the widespread industrial and residential applications of DC systems. Although DC systems are widely used and benefit power systems, the safety, reliability, and efficiency of DC systems are challenged by electrical faults [3]. Line-line faults, ground faults, overcurrent faults, and arc faults impede the normal operation of DC systems [2]. In particular, accidental arc faults can cause malfunctions and even lead to fire hazards in DC systems [4]. Arc faults can be classified into two types: series arc faults and parallel arc faults. A series arc fault is induced by the failure of the intended continuity of a conductor or connector while a parallel arc fault is due to the insulation breakdown between the parallel conductors. To prevent DC systems from arc hazards, arc-fault detection techniques and devices are indispensable. According to National Electrical Code 2011 section 690.11 of the United States, arc fault protection is required for photovoltaic (PV) systems with a maximum voltage higher than 80 V. The standard of PV arc-fault-circuit interrupters (AFCI) is stipulated by Underwriters Laboratories (UL) in UL 1699B and an AFCI must detect arc faults with powers larger than 300 W [5]. However,

Manuscript received October 14, 2020; accepted November 17, 2020. Date of publication December 1, 2020; date of current version February 5, 2021. This work was supported in part by the Seed Funding Program for Basic Research, in part by the Seed Funding Program for Applied Research, in part by the Small Project Funding Program from The University of Hong Kong, Hong Kong, in part by the Innovation and Technology Fund (ITF) Tier 3 Funding under Grant ITS/203/14, Grant ITS/104/13, and Grant ITS/214/14, in part by Research Grants Council-General Research Fund (RGC-GRF) under Grant HKU 17204617, in part by the University Grants Committee of Hong Kong under Contract AoE/P-04/08, and in part by the U.S. National Science Foundation under Grant ECCS-1824710. The associate editor coordinating the review of this article and approving it for publication was Prof. Tien-Kan Chung. *(Corresponding author: Philip W. T. Pong.)*

Wenchao Miao is with the School of Mechatronic Engineering and Automation, Shanghai University, Shanghai 200444, China.

Qi Xu and K. H. Lam are with the Department of Electrical and Electronic Engineering, The University of Hong Kong, Hong Kong.

Philip W. T. Pong is with the Department of Electrical and Computer Engineering, New Jersey Institute of Technology, Newark, NJ 07102 USA, and also with the Department of Electrical and Electronic Engineering, The University of Hong Kong, Hong Kong (e-mail: wp24@njit.edu).

H. Vincent Poor is with the Department of Electrical Engineering, Princeton University, Princeton, NJ 08544 USA.

Digital Object Identifier 10.1109/JSEN.2020.3041737

1558-1748 © 2020 IEEE. Personal use is permitted, but republication/redistribution requires IEEE permission.
See https://www.ieee.org/publications/rights/index.html for more information.

Authorized licensed use limited to: Princeton University. Downloaded on November 20,2021 at 22:03:44 UTC from IEEE Xplore. Restrictions apply.

the randomness and complexity of arc faults make it difficult to extract arc signatures and define their characteristics for arc-fault detection.

Generally, parallel arc faults provoking extra current paths and dramatic increase of current can be terminated by over-current protection devices such as fuses. Nevertheless, series arc faults introduce arc impedance into the system leading to the decline of current, and as a result, the conventional protection devices operated by excitation current may not be triggered [6]. Therefore, methodologies to detect series arc faults are of considerable interest and numerous studies have been carried out to investigate the characteristics of series arc faults for detection.

Currently, series arc-fault detection techniques are mainly based on the extraction and analysis of arc frequency signatures from the variations of current caused by arcing. Arc frequency signatures can be obtained from the arc current by the Fast Fourier Transform (FFT) to achieve discrimination between normal operation and arc faults [7], [8]. However, the FFT does not reflect time-domain information and thus the exact time of the occurrence of an arc fault cannot be found. The Short-Time Fourier Transform (STFT) has been adopted to obtain the arc signatures in the time-frequency domain [9]. A proper window length should be determined for the STFT to achieve a compromise between the resolution in the time and frequency domains, as otherwise the effectiveness of arc-fault detection may be impacted [10]. To ensure the high resolution of arc signatures in the time-frequency domain, the wavelet transform (WT) has been widely exploited [11]–[14]. There are also other arc-fault detection techniques. Arc features from the quantum probability model [15], cross-correlation function [16], and principal components of arc voltage and current [17] can be calculated to detect arc faults. In the time domain, voltage drop [18] and current fluctuation [19] can be utilized in arc-fault detection by using predefined thresholds. Antennas are used to capture the electromagnetic radiation emitted by arcing to identify the series arc faults [20]–[22], but the appearance of arc signatures varies from several MHz to 800 MHz.

Although the widely adopted methods based on arc-frequency signatures have been extensively studied, they may be susceptible to environmental noises and power electronics noise in a power system [10]. It is important to segregate the arc signatures and noises. A bandpass filter and WT can be used for denoising the arc signatures, but they require knowledge of the frequency range of interfering noises [11], [12]. Furthermore, methods such as the FFT, STFT, and WT detect arc faults by comparing arc signatures with predefined thresholds [10], [23], [24]. These thresholds vary with the operating conditions of the system, and thus they must be preset for each specific operating condition.

In this paper, a method based on empirical mode decomposition (EMD) with the analysis of the Hurst exponent (H) is developed to acquire arc time-frequency signatures despite the effects of power electronics noise. A high-pass filter with a cutoff frequency of 0.5 kHz is used to eliminate the DC component. The support vector machine (SVM) algorithm is adopted for decision making in arc-fault detection. It is verified that the proposed technique with EMD analysis can decompose the arc signatures from interfering noises by extracting the intrinsic frequency-energy oscillations with H of the intrinsic mode functions (IMFs) larger than 1/2. Unlike the arc-fault detection method based on the variational mode decomposition with analysis of Shannon entropy (Ep) which needs to predefine the threshold values of Ep [25], H being larger than 1/2 is used as a fixed selection criterion and does not vary with the operating conditions of the system. Though other machine learning tools have been applied in arc-fault detection [14], [26], the SVM performs better in solving a binary classification task [27] and it is shown here that the SVM can differentiate between normal operation and arc fault with higher accuracy than a decision tree or k-Nearest Neighbors. This proposed technique does not require knowledge of the frequency range of interference or predefining of different thresholds. An off-grid PV system as a typical DC system was implemented to test the proposed technique experimentally under various conditions. This proposed technique can detect arc faults effectively using the EMD based method and a simply trained SVM without suffering the effects of noises, load transient conditions, or the need for predefined thresholds.

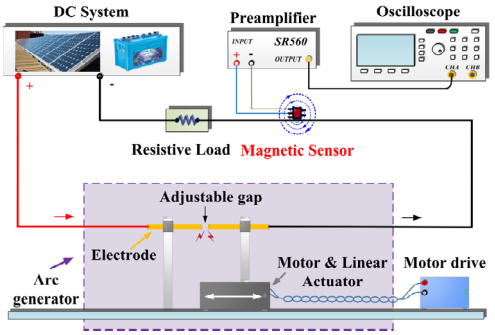

Fig. 1. An experimental setup for the generation of arc faults in DC systems.

This paper is organized as follows. In Section II, the extraction of arc signatures based on EMD is explained. In Section III, the algorithm based on SVM for distinguishing normal operation and arc faults is proposed. In Section IV, the experimental testing and validation of the proposed technique with the DC arc generator integrated with PV systems are discussed. Our conclusions are drawn in Section V.

II. Arc-Signature Extraction

A. DC Arc Generator

To investigate the characteristics of DC arc faults, a DC arc generator is developed as shown in Fig. 1. It can be series connected with a DC system and a resistive load to emulate the arc faults in a DC system. A voltage of 48 V is tested since 48 V is widely used in automotive, telecommunication, low-power loads, and DC-DC converter systems [28]–[30]. When the supply is around 48 V and 6 A, the minimum gap length to generate the arc fault is 0.4 mm and the gap length of 1 mm is too large to sustain an arc fault. The gap lengths of 0.4, 0.6, and 0.8 mm between the two copper electrodes

Authorized licensed use limited to: Princeton University. Downloaded on November 20,2021 at 22:03:44 UTC from IEEE Xplore. Restrictions apply.

are created by operating the stepper motor to induce series arc faults. The load current is measured by the magnetic sensor (TMR2001, MultiDimension) and the output of the TMR2001 is amplified by the preamplifier (SR560, Stanford Research Systems). The oscilloscope (MDO3014, Tektronix) is used to display the load current with a sampling rate of 250 kS/s. The frequency information up to 125 kHz of the load current can be acquired. The TMR sensor measures the current based on the magnetoresistance effect of a magnetic tunnel junction. The target current can be determined by the phenomenon that the electrical resistance of the TMR sensor changes as a function of the magnetic field generated from the current [31]. The TMR2001 is compact (less than 15 mm^3), low cost (approximately 1 USD per each), extremely low in power consumption (typically less than 0.4 mW) [32]. Hence, the TMR2001 is an excellent choice for detecting arc faults non-invasively and cost-effectively.

B. Characteristics of Arc Fault

Initially, a DC power supply was utilized as the power source of the arc generator for emulating arc faults. The TMR2001 sensor was pre-calibrated with the assistance of the current probe. The TMR2001 was fixed horizontally on the surface of the cable in diameter of 4 mm during the pre-calibration and experiments. The TMR2001 were tested with the current up to 10 A. The output voltage of the sensor varied linearly with the current and could be modeled by Eq. (1).

$$\boldsymbol{I_{TMR} = a_{TMR} \cdot V_{TMR} + b_{TMR}} \tag{1}$$

where I_{TMR} is the calibrated current, a_{TMR} and b_{TMR} depend on the features of TMR2001, V_{TMR} is the output voltage of TMR2001.

In this case, a_{TMR} and b_{TMR} were 4.01 and 1.59 respectively. The load current containing arc fault with a gap length of 0.6 mm was measured by the TMR2001 as shown in Fig. 2. The DC arc generator was operating in normal mode from 0 to 1.5 s and the load current was constant as Fig. 2 (a) depicts. The arc fault occurred at 1.5 s introducing arc impedance and noises to the system [33], [34]. Hence, the load current decreased and oscillated during the arcing. A selection window of 0.4 s was used to select the data of load current for analysis as shown in Fig. 2 (a). The power spectral density (PSD) of the current in normal operation and sustained arc was extracted by the FFT from the selected data as shown in Fig. 2 (b). In the presence of an arc fault, the PSD of the current increased apparently in the range from 0 to 125 kHz due to the noises generated by arcing. Thus, the arc faults can be detected by using this phenomenon [7], [8]. However, there are no time-domain signatures from the FFT. Therefore, the exact time of the occurrence of an arc fault could not be found causing difficulties in detecting arc faults simultaneously.

A bandpass filter, passing frequencies from 0.5 kHz to 100 kHz, could be used to obtain the frequency signatures of the arc current. Since the environmental noises are typically lower than 100 Hz [10], [26], the lower cutoff frequency of 0.5 kHz was high enough to exclude the environmental noises. In this way, the magnitude of arc signatures (I_{Arc}) can be

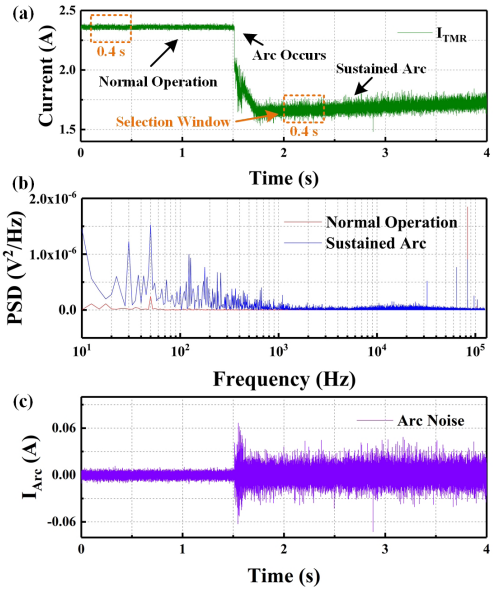

Fig. 2. The characteristics of the arc current measured by the TMR sensor. (a) Arc current in the time domain. (b) PSD of the current in normal operation and sustained arc. (c) Arc signatures from bandpass filter from 0.5 kHz to 100 kHz.

accurately determined and presented in the time domain as Fig. 2 (c) depicts. When the arc fault occurred at 1.5 s, the I_{Arc} increased dramatically. Therefore, the oscillatory behavior of the I_{Arc} induced by arcing from 0.5 kHz to 100 kHz can be utilized to distinguish the normal operation and arc faults in real-time.

C. Arc Signatures Decomposed by EMD

Though the arc frequency signatures from 0.5 kHz to 100 kHz can be used in arc fault detection, the operational frequencies of most power electronics are within this range and the electronic noises generated by power electronics can cause nuisance tripping to the arc fault detection. For example, the power electronics noise from the power supply and motor drive of the stepper motor existed in the arc current as shown in Fig. 3. The arc current at a gap length of 0.6 mm in the time domain is shown in Fig. 3 (a). In this case, the power electronics noise and arc signatures cannot be separated by using the FFT as depicted in Fig. 3 (b). The arc signatures interfered by the power electronics noise can lead to nuisance tripping. According to Fig. 3 (c), the power electronics noise is interfering with the arc signatures even after bandpass filtering from 0.5 kHz to 100 kHz.

To solve this problem, instead of using the bandpass filter or wavelet transform which requires knowledge of the frequency range of interfering noises, the method based on EMD is developed to decompose the arc signatures. The EMD treats a signal at the level of its local oscillations and can decompose the signal into a number of IMF and residual functions using the sifting process to obtain the local trends [35], [36]. The EMD analyzes the evolution of a signal $X(t)$ by tracing the local maxima and minima to construct an upper envelope $X_+(t)$ and a lower envelope $X_-(t)$. Then, the EMD computes

Authorized licensed use limited to: Princeton University. Downloaded on November 20,2021 at 22:03:44 UTC from IEEE Xplore. Restrictions apply.

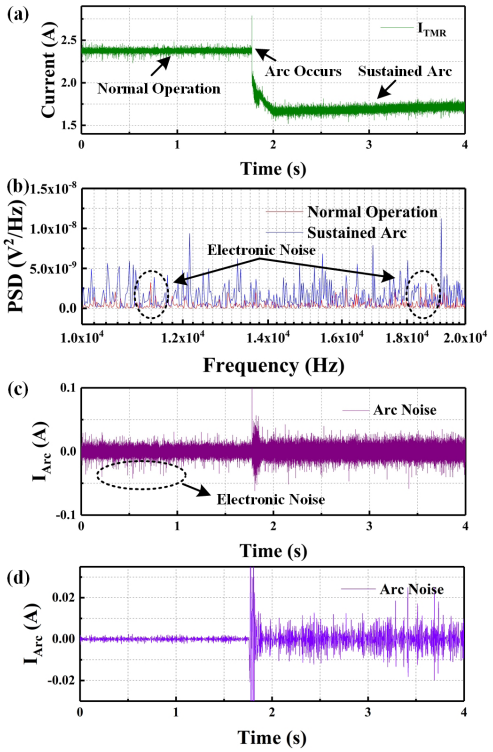

Fig. 3. The arc current with power electronics noise. (a) Current in the time domain. (b) PSD of the current. (c) Arc signatures after bandpass filtering from 0.5 kHz to 100 kHz. (d) Arc signatures decomposed by EMD analysis.

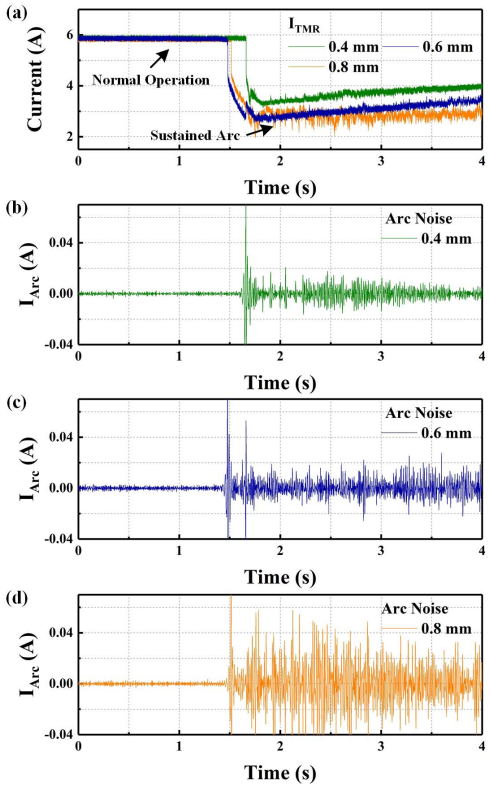

Fig. 4. The arc current generated at the gap length of 0.4, 0.6, and 0.8 mm and their signatures decomposed by the EMD analysis. (a) Arc current in the time domain. Arc signatures at (b) 0.4, (c) 0.6, and (d) 0.8 mm.

the mean envelope $m_{k,i}(t)$ by Eq. (2),

$$\boldsymbol{m_{k,i} = \left[X_+(t) + X_-(t)\right]/2} \tag{2}$$

where i is the number of the iteration, k is the number of IMF and residual functions.

Subtract the mean envelope from the $c_k(t)$ and $c_k(t) = X(t)$ for the first iteration,

$$\boldsymbol{c_k(t) = c_k(t) - m_{k,i}(t)} \tag{3}$$

When zero mean is extracted from the signal, the $c_k(t)$ can be regarded as an IMF.

When an IMF occurs, a new residual function is computed,

$$\boldsymbol{r_k(t) = r_{k-1}(t) - c_k(t)} \tag{4}$$

where $r_k(t)$ is the residual function.

Repeat Eq. (2) to (4) with the new residual function to find all IMFs. Finally, the signal $X(t)$ can be represented as,

$$\mathbf{X}(t) = \sum_{i=1}^{k} \boldsymbol{c_i(t) + r_k(t)} \tag{5}$$

To eliminate the interfering noises, the H of each IMF can be calculated by analyzing the variance progression of IMFs [36]. The H can be obtained by calculating the slope of $\log(R)$ against $\log(S)$.

$$\boldsymbol{H = (\log(R) - C)/\log(S)} \tag{6}$$

where R is the standard deviation (std) of the IMF $c(t)$, S is the function of the IMF number which is using [2^0, 2^1, $2^2 \ldots 2^k$] in this case, C is a constant.

The interfering noises can be denoised from the arc signatures by subtracting the IMFs with H lower than 1/2 from the arc signatures [36], [37]. The IMFs with H larger than 1/2 indicate the trend of intrinsic oscillations and most arc features can be retained in the IMFs. Thus, having an H larger than 1/2 is used as a fixed selection criterion in the EMD analysis for the extraction of arc signatures. This selection criterion does not vary with the operating conditions of the system. As shown in Fig. 3 (d), the arc signatures can still be successfully extracted by the EMD despite the effects of interfering noises. The DC component is filtered by the high-pass filter with a cutoff frequency of 0.5 kHz.

Although the noise level of an arc fault decreases with the gap length [38], the discrepancy between arcing and normal operation is typically unambiguous. This is confirmed by the arc faults at around 48 V with the gap lengths of 0.4, 0.6, and 0.8 mm as shown in Fig. 4. It can be seen from Fig. 4 (a) that the current decreased when the arc fault occurred and the arc current decreased with the gap length due to the increase of arc impedance. The arc time-frequency signatures at the gap length of 0.4, 0.6, and 0.8 mm are depicted in Fig 4 (b), (c), and (d) respectively. Though the magnitudes of the arc signatures decreased with the gap length, the oscillatory frequencies of arc fault at 0.4 mm decomposed by the EMD analysis were still large enough for detection.

The arc signatures in different current levels were also evaluated. The arc current and current noise in different current levels at a gap length of 0.6 mm are shown in Fig. 5.

Authorized licensed use limited to: Princeton University. Downloaded on November 20,2021 at 22:03:44 UTC from IEEE Xplore. Restrictions apply.

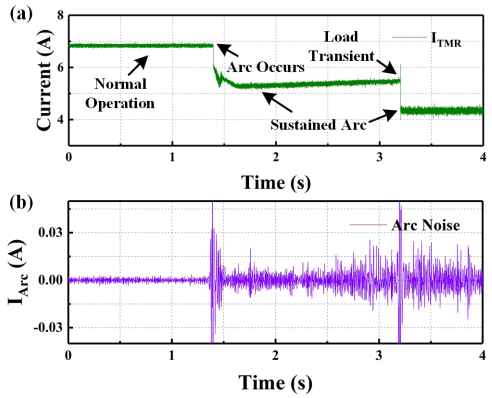

Fig. 5. The arc current at different current levels. (a) Arc current in the time domain. (b) Arc signatures decomposed by the EMD analysis.

The DC system was in normal operation until 1.39 s when the arc fault appeared. The resistance of load increased during arcing at 3.2 s resulting in the decrease of current as shown in Fig. 5 (a). It was confirmed that the arc signatures of different current levels can be effectively obtained by the proposed method based on EMD and the effectiveness would not be affected by the variation of arc current as shown in Fig. 5 (b). Therefore, the proposed method can facilitate the extraction of arc signatures despite the influences of load transients and power electronics noise.

D. Evaluation of EMD Analysis

The boundary effect, stopping criteria, and computational complexity of the EMD analysis are analyzed. In the proposed EMD analysis, the extrema are set close to edges by symmetry quality to reduce the errors due to the boundary effect. The sifting process is stopped satisfactorily only when the difference between the number of extrema and zero-crossings is less than 1 and the mean envelope close to zero [35], [39]. The amplitude of mean envelop are evaluated by comparison with the amplitude of the corresponding mode. In the EMD analysis, the stopping criteria based on two thresholds θ_1 and θ_2 are adopted to ensure the mean envelope has the globally small fluctuations and the locally large excursions are considered [39]. The mode amplitude is $a_{k,i}(t) = (X_+(t) - X_-(t))/2$ and the evaluation function is $\sigma_{k,i}(t) = |m_{k,i}(t)/a_{k,i}(t)|$. The sifting is stopped when $\sigma_{k,i}(t) < \theta_1$ for the fraction (1-α) of total duration and $\sigma_{k,i}(t) < \theta_2$ for the rest fraction. In this case, the θ_1 of 0.05, θ_2 of 0.5, and α of 0.05 are used. The time complexity of EMD is $41 \cdot N_s \cdot n \cdot n_m$ where N_s is the number of siftings, n is the data length, n_m is the number of IMFs, and $n_m = \log_2 n$. Since $41 \cdot N_s \cdot n \cdot (\log_2 n) = O(n \cdot \log n)$, the complexity of EMD is of the same order of FFT [40].

III. Algorithm Based on SVM

A. Feature Selection and Extraction for SVM

In this paper, instead of predefining thresholds for each operating condition of a system, the SVM was implemented for classifications of arc features and detections of arc faults. The arc features were analyzed and extracted by calculating

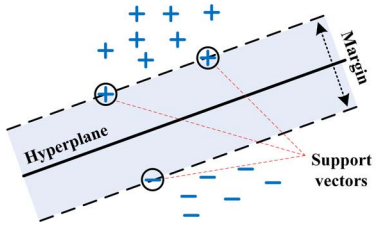

Fig. 6. The basic operational theory of SVM.

the energy (*Eg*), *Ep*, root-mean-square (*RMS*), and *std* of the arc signatures obtained by the proposed method. The *Eg* of the arc signatures can be calculated from Eq. (7).

$$Eg_i = \sum_{i=1}^{n} |S_{hi}|^2 \tag{7}$$

where S_h is the arc signal obtained from the proposed method.

The *Ep* indicating the uncertainty and complexity of the arc-noise signal can be expressed by Eq. (8).

$$Ep(S_h) = -\sum_{i} S_{hi}^2 \log(S_{hi}^2) \tag{8}$$

The *RMS* of the arc signatures (N_{RMS}) is given in Eq. (9).

$$N_{RMS} = \sqrt{\frac{1}{N} \sum_{i=1}^{N} |S_{hi}|^2} \tag{9}$$

The *std* of the arc signatures (N_{std}) is calculated by Eq. (10) as,

$$N_{std} = \sqrt{\frac{1}{N-1} \sum_{i=1}^{N} |S_{hi} - \mu|^2}$$
$$\mu = \frac{1}{N} \sum_{i=1}^{N} S_{hi} \tag{10}$$

where μ is the mean of S_h.

The arc features are utilized to train an SVM model so that the model can discriminate between normal operation and arc fault. The SVM algorithm can learn from data and solve classification and regression problems [27]. In particular, the SVM is useful for binary classification problems [27]. A linear SVM for two-class learning can separate the data by an optimal hyperplane as illustrated in Fig. 6. The optimal hyperplane realizes the largest margin between the two classes of data '+' and '−'. The margin means the maximal width of the parallel-to-hyperplane slab with no interior data points. The data points on the boundary of the slab are regarded as support vectors. The equation of the hyperplane is express in Eq. (11).

$$W^T x_i + b = 0 \tag{11}$$

where W is the adjustable weight vector, x_i is the input features, and b is the bias of hyperplane. The separable case can be represented as Eq. (12).

$$W^T x_i + b \le 0 \quad \text{for } d_i = -$$
$$W^T x_i + b > 0 \quad \text{for } d_i = + \tag{12}$$

where d_i is the classification output.

Authorized licensed use limited to: Princeton University. Downloaded on November 20,2021 at 22:03:44 UTC from IEEE Xplore. Restrictions apply.

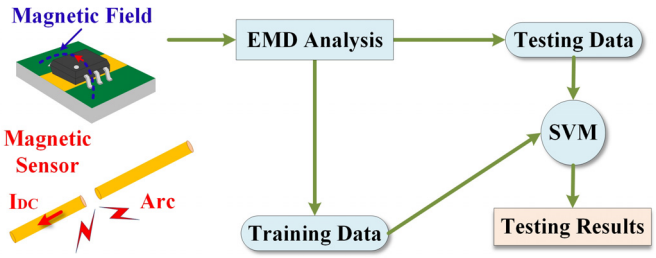

Fig. 7. The procedures of arc-fault detection.

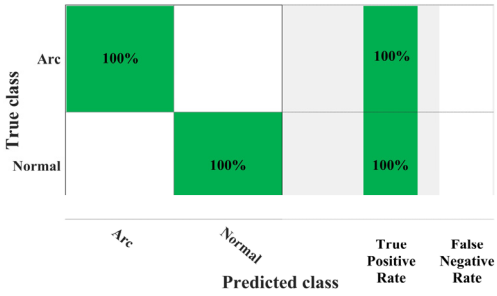

Fig. 8. The confusion matrix of the training results.

B. Proposed Detection Methodology

An online arc-fault detection system was developed as Fig. 7 depicts. As explained in Section II, magnetic field sensing can be carried out by magnetoresistive sensors such as the TMR2001 to sense the current for arc-fault detection. The proposed method based on EMD can acquire the arc signatures from the arc current of the target DC system to train the SVM model. The training data could be collected from the typical potential arc faults of the DC system. The background and intrinsic power electronics noise of the DC system can be eliminated by the proposed method based on EMD analysis to prevent the nuisance tripping. Therefore, in the occurrence of an arc fault, the arc signatures can be obtained accurately using the proposed method. The arc fault can be detected by identifying the arc signatures with the trained SVM model. The training results of the arc signatures from the arc current with power electronics noise in the DC arc generator are shown in Fig. 8. The confusion matrix verifies that the arc signatures can be exactly classified by the linear SVM with an accuracy of 100%. The arc faults at various current levels and during load transient conditions were also emulated in the DC arc generator to test the trained linear SVM model. The testing results demonstrated that the linear SVM model discriminated between the normal operations and arc faults with accuracies larger than 99.4%. The linear SVM can be used for decision making in arc-fault detection. Therefore, a reliable arc-fault detection system can be developed by using the TMR sensor, EMD analysis, and SVM.

IV. Validation in PV System

To test and validate the proposed method in a typical DC system, an off-grid PV system was developed. A PV simulator was used to emulate the operation of PV panels under various irradiance and temperature conditions. The arc-fault detection system was used to determine arc faults at different gap lengths, current levels, and also during load transient conditions. The influence of the power electronics noise from the maximum power point tracking (MPPT) controller and inverter to the detection system was also studied and analyzed.

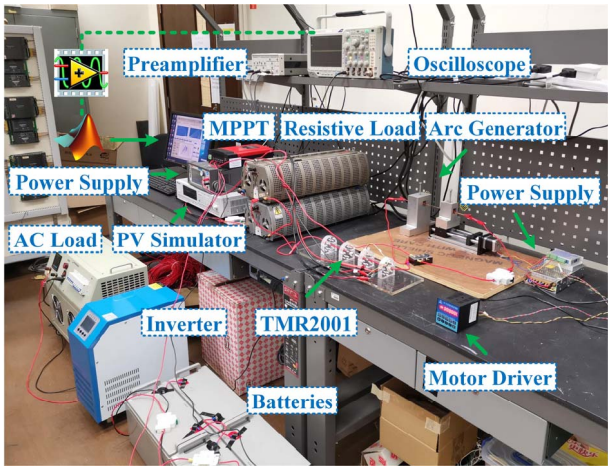

Fig. 9. The experimental setup of an off-grid PV system.

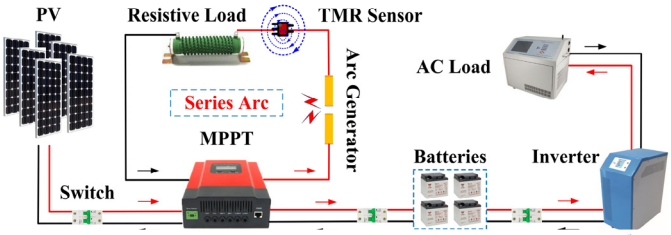

Fig. 10. The schematic of the PV system integrated with the DC arc generator.

A. Experimental Setup

The off-grid PV system integrated with the DC arc generator consists of a computer, a PV simulator, an MPPT controller, batteries, an inverter, an AC load, and resistive loads as presented in Fig. 9. The schematic of the system is illustrated in Fig. 10. The PV simulator (62020H-150S, Chroma) emulated the PV system in different irradiance and temperature levels. The MPPT controller harvested the maximal power to charge the batteries and supply the resistive loads. The inverter inverted the power from DC to AC for the consumption of the AC load. To investigate the capability of the arc-fault detection system, the arc generator was placed between the MPPT and resistive loads. The TMR2001 measured the load current and the output of TMR2001 was amplified by the preamplifier. The load current measured by TMR2001 could be obtained from the oscilloscope to the computer through the LabVIEW. The proposed method extracted the arc signatures for the SVM to differentiate between normal operations and arc faults.

B. Experimental Results and Discussion

The real-world irradiance and temperature levels of a day in Hong Kong provided by the Hong Kong Observatory were imported to the PV simulator as depicted in Fig. 11. It emulated the operation of a PV system with the voltage of 100 V. The AC load was switched to the resistive mode of 100 W. The arc faults were induced by the arc generator

Authorized licensed use limited to: Princeton University. Downloaded on November 20,2021 at 22:03:44 UTC from IEEE Xplore. Restrictions apply.

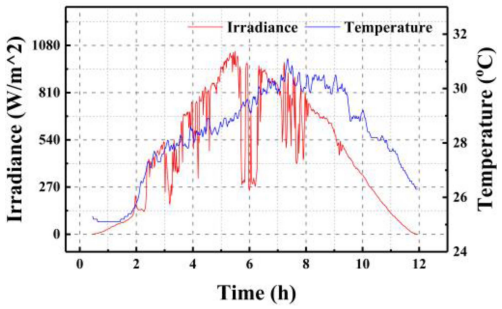

Fig. 11. The irradiance and temperature levels of a typical day in Hong Kong.

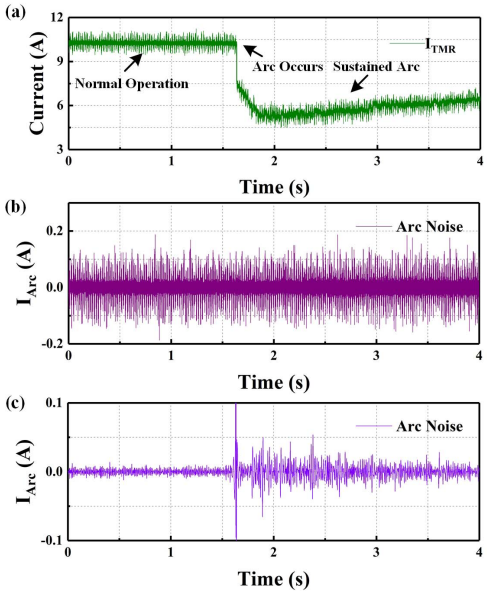

Fig. 12. Arc current at the gap length of 0.4 mm in the PV system. (a) Current in the time domain. (b) Arc signatures extracted by the bandpass filter from 0.5 kHz to 100 kHz. (c) Arc signatures decomposed by the EMD analysis.

which was supplied by the MPPT controller. Initially, the arc fault was generated at the load current of around 10 A during the normal operation at a gap length of 0.4 mm as shown in Fig. 12 (a). The arc signatures extracted by the bandpass filter from 0.5 kHz to 100 kHz are shown in Fig. 12 (b). Since the MPPT controller operating at 50 kHz and the inverter at 20 kHz introduced power electronics noise to the system, the clarity of arc signatures from 0.5 kHz to 100 kHz was deteriorated. Moreover, there was power electronics noise from the motor driver and power supply. The proposed method based on EMD could acquire the arc signatures successfully as depicted in Fig. 12 (c). Then, the arc features were calculated and applied as training data for linear SVM built with MATLAB.

In each test, the current of 4 s was captured and 100 k points were selected for analysis. For the arc signatures, 200 points of the current in 8 ms were used to calculate each sample and there were 500 samples per test. Since four parameters of arc features were calculated, there were 2000 features in the training data set. The training results verified that the arc features of the PV system could be classified by the linear SVM with an accuracy of 98.8% as depicted in Fig. 13. It was

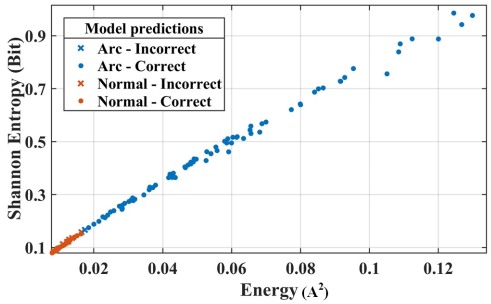

Fig. 13. The classifications of the training data by the linear SVM model.

Fig. 14. The classification accuracies of the decision tree, k-Nearest Neighbors, and linear SVM.

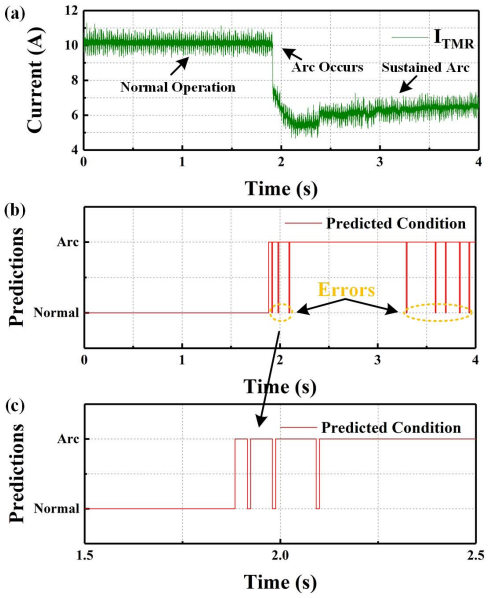

Fig. 15. The predicted condition of the PV system with the arc fault at a gap length of 0.4 mm. (a) Arc current in the time domain from 0 to 4 s. (b) Predicted conditions of the PV system from 0 to 4 s in a step of 8 ms and (c) zoomed-in results from 1.5 to 2.5 s.

found that the SVM could achieve a higher classification accuracy than other tools such as the decision tree (93.8%) and the *k*-Nearest Neighbors (95.0%) as shown in Fig. 14.

To test the trained SVM model, another arc fault with a gap length of 0.4 mm at 10 A was generated as shown in Fig. 15 (a). The trained SVM model could output the condition of the PV system in a step of 8 ms as depicted in Fig. 15 (b) and (c). The misjudgments did not continuously occur twice and could be avoided by checking the prediction results of three consecutive intervals. An arc fault could be determined when the condition of the PV system was predicted as 'arc' in two consecutive intervals or 'arc' was predicted twice in three consecutive intervals. Besides,

Authorized licensed use limited to: Princeton University. Downloaded on November 20,2021 at 22:03:44 UTC from IEEE Xplore. Restrictions apply.

TABLE I
TESTING RESULTS WITH ARC FAULT AT A GAP LENGTH OF 0.4 mm

Case	Test	Accuracy (%)
Arc faults at the current of 10 A	50	98
Arc faults at the current of 5 A	50	100
Arc faults at the current from 10 to 5 A	50	96

TABLE II
TESTING RESULTS WITH ARC FAULT AT A GAP LENGTH OF 0.6 mm

Case	Test	Accuracy (%)
Arc faults at the current of 10 A	50	100
Arc faults at the current of 5 A	50	100
Arc faults at the current from 10 to 5 A	50	98

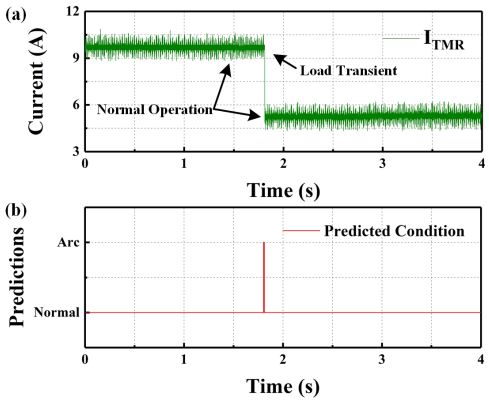

Fig. 16. The predicted condition of the PV system in load transient condition. (a) Current during load transient in the time domain. (b) Predicted conditions.

the computational time was approximately 15.6 ms for each prediction. Thus, the arc fault could be determined within three consecutive intervals in about 70.8 ms.

The SVM model was further examined with arc faults in the current levels of about 5 A and also arc faults during the current decreased from 10 to 5 A. The testing results of the three cases based on three consecutive prediction results are provided in Table I. In each case, a group of 50 arc faults was emulated for testing and the minimum accuracy was 96%. Similarly, the arc faults of the three cases at a gap length of 0.6 and 0.8 mm were tested. The results are presented in Table II and III respectively. The experimental results verified that the minimum accuracy of all the tests was 96%. Besides, the performance of the trained model under load transient condition in normal operation was studied as depicted in Fig. 16 (a) and (b). There was only one misjudgment that occurred when the load transient started. Therefore, it can be concluded that the proposed arc-fault detection system based on the EMD analysis and SVM can identify arc faults in the PV system with a minimum accuracy of 96% and a detection speed of 70.8 ms at different gap lengths and current levels despite the effects of power electronics noise and transient conditions.

Since the arc-fault detection methods may be impacted by the power electronics noise and postponed arc-fault detection can cause malfunction to the system, numerous investigations have been carried out to develop a reliable and high-speed arc-fault detection technique. The method based on WT can detect the arc faults emulated from a simplified DC system with an accuracy of 100% excluding the high power level [11].

TABLE III
TESTING RESULTS WITH ARC FAULT AT A GAP LENGTH OF 0.8 mm

Case	Test	Accuracy (%)
Arc faults at the current of 10 A	50	100
Arc faults at the current of 5 A	50	100
Arc faults at the current from 10 to 5 A	50	100

However, it requires knowledge of the bandwidth of interfering noises and the detection time is about 100 ms. Besides, it takes approximately 0.5 s for a guaranteed detection of an arc fault based on the arc current entropy calculated by the quantum probability model [15]. The detection accuracy based on the Wigner-Ville distribution with the interference of power electronics noise is 87.19% and the data in a period of 40 ms is needed [6]. Therefore, the proposed method based on EMD analysis and SVM is a competitive candidate for DC arc-fault detection.

C. Implementation and Future Work

Since the proposed method is based on magnetic-field sensing of the arc current, only one magnetic sensor is required for the target branch of a DC system. For instance, in a PV system, the arc time-frequency signatures can be captured by placing a magnetic sensor on the power cable of each PV string. Within the PV string, there is no particular requirement for the location of the magnetic sensor as the arc time-frequency signatures are contained in the current flowing through the entire PV string. Besides, the PV strings are merged inside the PV array combiner box and magnetic sensors can be installed inside the combiner box for better protection. The expense of installing a magnetic sensor for each PV string is low by using the TMR2001. However, in other DC systems, the interfering noises may vary with branches and the typical arc signatures from different branches should be obtained to train the SVM model. In future work, a digital signal processor (DSP) or a field-programmable gate array (FPGA) can be adopted to realize the decomposition of arc signatures by the proposed EMD analysis [41]. The FPGA can also be used for the hardware implementation of SVM [42]. Therefore, a DC arc-fault detection system can be developed by installing the TMR2001 on each branch of a DC system to sense the current and using the FPGA and DSP to achieve the proposed EMD analysis and SVM. The reliability and efficiency of the arc-fault detection system will be examined in other DC systems.

V. CONCLUSION

In this paper, a series DC arc-fault detection system based on the EMD analysis and using SVM in decision making has been developed. The proposed technique was tested at 48 V with a gap length of 0.4, 0.6, and 0.8 mm. The testing current was higher than 6 A in constant and also transient conditions. It was verified that the EMD method can acquire the arc signatures during these conditions and despite the effect

Authorized licensed use limited to: Princeton University. Downloaded on November 20,2021 at 22:03:44 UTC from IEEE Xplore. Restrictions apply.

of power electronics noise. The technique test experimentally in an off-grid PV system, and the results demonstrated that the technique was capable of series arc-fault detection at gap lengths of 0.4, 0.6, and 0.8 mm and current levels of 10 A, 5 A, and from 10 A to 5 A despite the interference of power electronics noise. According to the experimental results, the lowest detection accuracy of the technique was 96% for a testing group of 50 arc faults. In practical implementations, the compact, non-invasive and low-cost magnetic sensors such as TMR2001 can be used for sensing the arc current non-invasively.

REFERENCES

[1] E. Rodriguez-Diaz, J. C. Vasquez, and J. M. Guerrero, "Intelligent DC homes in future sustainable energy systems: When efficiency and intelligence work together," *IEEE Consum. Electron. Mag.*, vol. 5, no. 1, pp. 74–80, Jan. 2016.

[2] S. Beheshtaein, R. M. Cuzner, M. Forouzesh, M. Savaghebi, and J. M. Guerrero, "DC microgrid protection: A comprehensive review," *IEEE J. Emerg. Sel. Topics Power Electron.*, early access, Mar. 12, 2019, doi: 10.1109/JESTPE.2019.2904588.

[3] J.-D. Park and J. Candelaria, "Fault detection and isolation in low-voltage DC-bus microgrid system," *IEEE Trans. Power Del.*, vol. 28, no. 2, pp. 779–787, Apr. 2013.

[4] D. S. Pillai and N. Rajasekar, "A comprehensive review on protection challenges and fault diagnosis in PV systems," *Renew. Sustain. Energy Rev.*, vol. 91, pp. 18–40, Aug. 2018.

[5] *Outline of Investigation for Photovoltaic DC Arc-Fault Circuit Protection*, Standard UL1699B, Underwriters Laboratories, 2011.

[6] S. Chen, X. Li, Z. Xie, and Y. Meng, "Time–frequency distribution characteristic and model simulation of photovoltaic series arc fault with power electronic equipment," *IEEE J. Photovolt.*, vol. 9, no. 4, pp. 1128–1137, Jul. 2019.

[7] J. Johnson *et al.*, "Differentiating series and parallel photovoltaic arc-faults," in *Proc. 38th IEEE Photovoltaic Specialists Conf.*, Jun. 2012, pp. 000720–000726.

[8] J.-C. Gu, D.-S. Lai, J.-M. Wang, J.-J. Huang, and M.-T. Yang, "Design of a DC series arc fault detector for photovoltaic system protection," *IEEE Trans. Ind. Appl.*, vol. 55, no. 3, pp. 2464–2471, Jun. 2019.

[9] S. Chen, X. Li, and J. Xiong, "Series arc fault identification for photovoltaic system based on time-domain and time-frequency-domain analysis," *IEEE J. Photovolt.*, vol. 7, no. 4, pp. 1105–1114, Jul. 2017.

[10] S. Lu, B. T. Phung, and D. Zhang, "A comprehensive review on DC arc faults and their diagnosis methods in photovoltaic systems," *Renew. Sustain. Energy Rev.*, vol. 89, pp. 88–98, Jun. 2018.

[11] X. Yao, L. Herrera, S. Ji, K. Zou, and J. Wang, "Characteristic study and time-domain discrete- wavelet-transform based hybrid detection of series DC arc faults," *IEEE Trans. Power Electron.*, vol. 29, no. 6, pp. 3103–3115, Jun. 2014.

[12] Z. Wang and R. S. Balog, "Arc fault and flash signal analysis in DC distribution systems using wavelet transformation," *IEEE Trans. Smart Grid*, vol. 6, no. 4, pp. 1955–1963, Jul. 2015.

[13] C. He, L. Mu, and Y. Wang, "The detection of parallel arc fault in photovoltaic systems based on a mixed criterion," *IEEE J. Photovolt.*, vol. 7, no. 6, pp. 1717–1724, Nov. 2017.

[14] R. D. Telford, S. Galloway, B. Stephen, and I. Elders, "Diagnosis of series DC arc faults—A machine learning approach," *IEEE Trans. Ind. Informat.*, vol. 13, no. 4, pp. 1598–1609, Aug. 2017.

[15] N. L. Georgijevic, M. V. Jankovic, S. Srdic, and Z. Radakovic, "The detection of series arc fault in photovoltaic systems based on the arc current entropy," *IEEE Trans. Power Electron.*, vol. 31, no. 8, pp. 5917–5930, Aug. 2016.

[16] M. Ahmadi, H. Samet, and T. Ghanbari, "Series arc fault detection in photovoltaic systems based on signal-to-noise ratio characteristics using cross-correlation function," *IEEE Trans. Ind. Informat.*, vol. 16, no. 5, pp. 3198–3209, May 2020.

[17] M. Ahmadi, H. Samet, and T. Ghanbari, "A new method for detecting series arc fault in photovoltaic systems based on the blind-source separation," *IEEE Trans. Ind. Electron.*, vol. 67, no. 6, pp. 5041–5049, Jun. 2020.

[18] A. Shekhar, L. Ramirez-Elizondo, S. Bandyopadhyay, L. Mackay, and P. Bauera, "Detection of series arcs using load side voltage drop for protection of low voltage DC systems," *IEEE Trans. Smart Grid*, vol. 9, no. 6, pp. 6288–6297, Nov. 2018.

[19] M. Naidu, T. J. Schoepf, and S. Gopalakrishnan, "Arc fault detection scheme for 42-V automotive DC networks using current shunt," *IEEE Trans. Power Electron.*, vol. 21, no. 3, pp. 633–639, May 2006.

[20] C. J. Kim, "Electromagnetic radiation behavior of low-voltage arcing fault," *IEEE Trans. Power Del.*, vol. 24, no. 1, pp. 416–423, Jan. 2009.

[21] S. Zhao, Y. Wang, F. Niu, C. Zhu, Y. Xu, and K. Li, "A series DC arc fault detection method based on steady pattern of high-frequency electromagnetic radiation," *IEEE Trans. Plasma Sci.*, vol. 47, no. 9, pp. 4370–4377, Sep. 2019.

[22] Q. Xiong *et al.*, "Electromagnetic radiation characteristics of series DC arc fault and its determining factors," *IEEE Trans. Plasma Sci.*, vol. 46, no. 11, pp. 4028–4036, Nov. 2018.

[23] M. K. Alam, F. Khan, J. Johnson, and J. Flicker, "A comprehensive review of catastrophic faults in PV arrays: Types, detection, and mitigation techniques," *IEEE J. Photovolt.*, vol. 5, no. 3, pp. 982–997, May 2015.

[24] S. Chae, J. Park, and S. Oh, "Series DC arc fault detection algorithm for DC microgrids using relative magnitude comparison," *IEEE J. Emerg. Sel. Topics Power Electron.*, vol. 4, no. 4, pp. 1270–1278, Dec. 2016.

[25] S. Liu, L. Dong, X. Liao, X. Cao, X. Wang, and B. Wang, "Application of the variational mode decomposition-based time and time–frequency domain analysis on series DC arc fault detection of photovoltaic arrays," *IEEE Access*, vol. 7, pp. 126177–126190, 2019.

[26] S. Lu, T. Sirojan, B. T. Phung, D. Zhang, and E. Ambikairajah, "DA-DCGAN: An effective methodology for DC series arc fault diagnosis in photovoltaic systems," *IEEE Access*, vol. 7, pp. 45831–45840, 2019.

[27] R. K. Begg, M. Palaniswami, and B. Owen, "Support vector machines for automated gait classification," *IEEE Trans. Biomed. Eng.*, vol. 52, no. 5, pp. 828–838, May 2005.

[28] E. Rodriguez-Diaz, F. Chen, J. C. Vasquez, J. M. Guerrero, R. Burgos, and D. Boroyevich, "Voltage-level selection of future two-level LVdc distribution grids: A compromise between grid compatibiliy, safety, and efficiency," *IEEE Electrific. Mag.*, vol. 4, no. 2, pp. 20–28, Jun. 2016.

[29] F. Chen, R. Burgos, and D. Boroyevich, "A bidirectional high-efficiency transformerless converter with common-mode decoupling for the interconnection of AC and DC grids," *IEEE Trans. Power Electron.*, vol. 34, no. 2, pp. 1317–1333, Feb. 2019.

[30] A. Frances-Roger, A. Anvari-Moghaddam, E. Rodriguez-Diaz, J. C. Vasquez, J. M. Guerrero, and J. Uceda, "Dynamic assessment of COTS converters-based DC integrated power systems in electric ships," *IEEE Trans. Ind. Informat.*, vol. 14, no. 12, pp. 5518–5529, Dec. 2018.

[31] J. Lenz and S. Edelstein, "Magnetic sensors and their applications," *IEEE Sensors J.*, vol. 6, no. 3, pp. 631–649, Jun. 2006.

[32] *MultiDimension TMR2001*. Accessed: Oct. 10, 2020. [Online]. Available: http://www.dowaytech.com/en/index.php?c=download&id=2025

[33] J. Keenan and M. Parker, "Arc detectors," in *Proc. 20th Int. Telecommun. Energy Conf.*, 1998, pp. 710–715.

[34] F. Schimpf and L. E. Norum, "Recognition of electric arcing in the DC-wiring of photovoltaic systems," in *Proc. 31st Int. Telecommun. Energy Conf. (INTELEC)*, Oct. 2009, pp. 1–6.

[35] N. E. Huang *et al.*, "The empirical mode decomposition and the Hilbert spectrum for nonlinear and non-stationary time series analysis," *Proc. Roy. Soc. London. A, Math., Phys. Eng. Sci.*, vol. 454, no. 1971, pp. 903–995, Mar. 1998.

[36] P. Flandrin, G. Rilling, and P. Goncalves, "Empirical mode decomposition as a filter bank," *IEEE Signal Process. Lett.*, vol. 11, no. 2, pp. 112–114, Feb. 2004.

[37] P. Flandrin, P. Gonçalvès, and G. Rilling "Detrending and denoising with empirical mode decompositions," in *Proc. 12th Eur. Signal Process. Conf.*, Sep. 2004, pp. 1581–1584.

[38] W. Miao, X. Liu, K. H. Lam, and P. W. T. Pong, "Arc-faults detection in PV systems by measuring pink noise with magnetic sensors," *IEEE Trans. Magn.*, vol. 55, no. 7, pp. 1–6, Jul. 2019.

[39] G. Rilling, P. Flandrin, and P. Goncalves, "On empirical mode decomposition and its algorithms," in *Proc. IEEE-EURASIP Workshop Nonlinear Signal Image Process.*, vol. 3, no. 3, pp. 8–11, Jun. 2003.

[40] Y.-H. Wang, C.-H. Yeh, H.-W.-V. Young, K. Hu, and M.-T. Lo, "On the computational complexity of the empirical mode decomposition algorithm," *Phys. A, Stat. Mech. Appl.*, vol. 400, pp. 159–167, Apr. 2014.

[41] M.-H. Lee, K.-K. Shyu, P.-L. Lee, C.-M. Huang, and Y.-J. Chiu, "Hardware implementation of EMD using DSP and FPGA for online signal processing," *IEEE Trans. Ind. Electron.*, vol. 58, no. 6, pp. 2473–2481, Jun. 2011.

[42] R. Saini, S. Saurav, D. C. Gupta, and N. Sheoran, "Hardware implementation of SVM using system generator," in *Proc. 2nd IEEE Int. Conf. Recent Trends Electron., Inf. Commun. Technol. (RTEICT)*, May 2017, pp. 2129–2132.

Authorized licensed use limited to: Princeton University. Downloaded on November 20,2021 at 22:03:44 UTC from IEEE Xplore. Restrictions apply.

Wenchao Miao received the B.Eng. degree from the University of Nottingham in 2014, the M.Sc. degree from The University of Manchester in 2016, and the Ph.D. degree in electrical and electronic engineering from The University of Hong Kong in 2020. He is currently a Lecturer with the School of Mechatronic Engineering and Automation, Shanghai University. His current research interests include application of magnetoresistive sensors in power systems, faults detection in dc systems, and condition monitoring of photovoltaic systems.

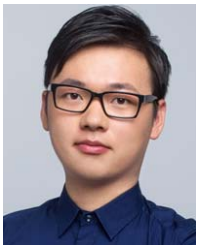

Qi Xu received the B.Eng. degree from Dalian Maritime University, Dalian, China, in 2018. He is currently pursuing the Ph.D. degree with the Department of Electrical and Electronic Engineering, The University of Hong Kong, Hong Kong. His research interests include non-intrusive fault detection, machine learning, and applications of magnetic sensors in microgrids.

K. H. Lam received the bachelor's degree in electrical energy systems engineering and the Ph.D. degree in architecture from The University of Hong Kong, in 1994 and 2007, respectively. He worked with the building services industry after graduation and returned to his Alma Mater joining the HKU Photovoltaic Research Team, in 1998. He worked as a Senior Manager with Solar Energy Company. From 2008 to 2009, he was the Chairman of the Hong Kong Photovoltaic Consortium. He was appointed as a Lecturer with the Department of Electrical and Electronic Engineering, The University of Hong Kong in 2014, where he was an Honorary Assistant Professor, in 2016. He is currently a Lecturer with The University of Hong Kong. His current research interest includes photovoltaic systems integration. He is also a Registered Chartered Electrical Engineer with the Engineering Council, U.K., and a Registered Energy Assessor with the Hong Kong Government.

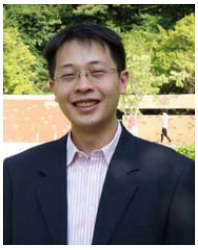

Philip W. T. Pong (Senior Member, IEEE) received the B.Eng. (Hons.) degree from The University of Hong Kong in 2002, and the Ph.D. degree in engineering from the University of Cambridge. He was a Postdoctoral Researcher with the Magnetic Materials Group, National Institute of Standards and Technology, USA, for a period of three years. His current research interest includes development and application of advanced sensing techniques-based on electromagnetic sensors in smart grid and nanotechnology. He is a Fellow of the Institution of Engineering and Technology (FIET), a Fellow of the Energy Institute (FEI), a Fellow of the Institute of Materials, Minerals and Mining (FIMMM), a Fellow of the NANOSMAT Society (FNS), a Chartered Physicist (CPhys), a Chartered Electrical Engineer (CEng), a Chartered Energy Engineer, a Registered Professional Engineer (R.P.E. in Electrical, Electronics, Energy), and a Corporate Member of HKIE (MHKIE in Electrical, Electronics, Energy). He serves on the editorial boards for several IEEE and SCI journals.

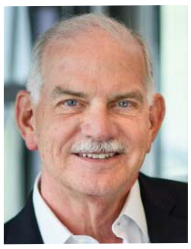

H. Vincent Poor (Life Fellow, IEEE) received the Ph.D. degree in EECS from Princeton University in 1977.

From 1977 to 1990, he was on the faculty of the University of Illinois at Urbana–Champaign. Since 1990, he has been on the faculty at Princeton University, where he is the Michael Henry Strater University Professor of Electrical Engineering. From 2006 to 2016, he was the Dean of the Princeton's School of Engineering and Applied Science. He has also held visiting appointments at several other institutions, including most recently at Berkeley and Cambridge. His research interests include information theory, machine learning, and network science, and their applications in wireless networks, energy systems and related fields. Among his publications in these areas is the forthcoming book *Advanced Data Analytics for Power Systems* (Cambridge University Press, 2021). Dr. Poor is a member of the National Academy of Engineering and the National Academy of Sciences, and he is a foreign member of the Chinese Academy of Sciences, the Royal Society, and other national and international academies. Recent recognition of his work includes the 2017 IEEE Alexander Graham Bell Medal and the 2019 ASEE Benjamin Garver Lamme Award.

Authorized licensed use limited to: Princeton University. Downloaded on November 20,2021 at 22:03:44 UTC from IEEE Xplore. Restrictions apply.